RSC Advances

PAPER

View Article Online
View Journal | View Issue

Cite this: *RSC Adv.*, 2022, **12**, 19115

Electronic structure and interface contact of two-dimensional van der Waals boron phosphide/Ga_2SSe heterostructures†

Hoang-Thinh Do,[ab] Tuan V. Vu,[c] A. A. Lavrentyev,[d] Nguyen Q. Cuong,[ef] Pham V. Cuong[g] and Hien D. Tong*[h]

In this work, we systematically examine the electronic features and contact types of van der Waals heterostructures (vdWHs) combining single-layer boron phosphide (BP) and Janus Ga_2SSe using first-principles calculations. Owing to the out-of-plane symmetry being broken, the BP/Ga_2SSe vdWHs are divided into two different stacking patterns, which are BP/SGa_2Se and BP/$SeGa_2S$. Our results demonstrate that these stacking patterns are structurally and mechanically stable. The combination of single-layer BP and Janus Ga_2SSe gives rise to an enhancement in the Young's modulus compared to the constituent monolayers. Furthermore, at the ground state, the BP/Ga_2SSe vdWHs possess a type-I (straddling) band alignment, which is desired for next-generation optoelectronic applications. The interlayer separation and electric field are effectively used to tune the electronic features of the BP/Ga_2SSe vdWH from the type-I to type-II band alignment, and from semiconductor to metal. Our findings show that the BP/Ga_2SSe vdWH would be appropriate for next-generation multifunctional optoelectronic and photovoltaic devices.

Received 30th April 2022
Accepted 12th June 2022

DOI: 10.1039/d2ra02748h

rsc.li/rsc-advances

1 Introduction

In recent years, the search for novel materials has attracted much attention because of their unusual physical and chemical properties, which are appropriate for future high-performance nanoelectronic and optoelectronic devices. Recently, novel two-dimensional materials (2DMs) have appeared as promising candidates for novel optoelectronic and photocatalytic applications, owing to their extraordinary electronic properties and suitable band gaps.[1,2] At first, one of the most popular 2DMs, graphene, was successfully exfoliated[3] and received much attention owing to its high carrier mobility[4] and massive Dirac fermions.[5] Unfortunately, the lack of a band gap in graphene has limited its applications in high-speed devices, such as logical circuits and field-effect transistors.[6] Recently, there have been different strategies that can be used to open a sizable band gap in graphene, such as doping,[7] functionalization,[8] use of substrates,[9] and so on. Alongside these strategies, scientists are seeking novel graphene-like 2DMs, such as phosphorene,[10] transition metal dichalcogenides (TMDCs),[11] MXenes,[12,13] and so on. Unlike graphene, these 2DMs mostly possess semiconducting characteristics, thus they are suitable for optoelectronic and photocatalytic applications. Regarding the promising unique properties of 2DMs, the search for novel 2DMs remains challenging.

Very recently, single-layer boron phosphide (BP) has been successfully synthesized on sapphire or silicon substrates[14,15] and its properties predicted using different theoretical calculations.[16,17] It is obvious that single-layer BP is a semiconductor with a direct band gap of about 1.0–2.0 eV, depending on the measurement approaches.[18,19] Single-layer BP shows high carrier mobilities (over 10^4 cm^2 V^{-1} s^{-1}),[20] which are comparable with those in graphene (10^5 cm^2 V^{-1} s^{-1}).[21] The electronic, magnetic and transport properties of single-layer BP can be modulated by doping[22,23] and applying an electric field.[24] These controllable characteristics make single-layer BP a promising competitor for future applications.

Following the successful synthesis of a Janus MoSSe structure from MoS_2 and $MoSe_2$ monolayers,[25,26] many different 2D Janus structures have also been predicted and synthesized,

[a]*Division of Computational Mechatronics, Institute for Computational Science, Ton Duc Thang University, Ho Chi Minh City, Vietnam. E-mail: dohoangthinh@tdtu.edu.vn*

[b]*Faculty of Electrical and Electronics Engineering, Ton Duc Thang University, Ho Chi Minh City, Vietnam*

[c]*Division of Computational Physics, Institute for Computational Science, Ton Duc Thang University, Ho Chi Minh City, Vietnam*

[d]*Department of Electrical Engineering and Electronics, Don State Technical University, 1 Gagarin Square, 344010 Rostov-on-Don, Russian Federation*

[e]*Institute of Research and Development, Duy Tan University, Da Nang 550000, Vietnam*

[f]*Faculty of Natural Sciences, Duy Tan University, Da Nang 550000, Vietnam*

[g]*Faculty of Electrical Engineering Technology, Ha Noi University of Industry, Ha Noi 100000, Vietnam*

[h]*Faculty of Engineering, Vietnamese-German University, Binh Duong, Vietnam. E-mail: hien.td@vgu.edu.vn*

† Electronic supplementary information (ESI) available. See https://doi.org/10.1039/d2ra02748h

including Janus ZrSSe,[27] Janus PtSSe,[28,29] Janus $Pd_4S_3Se_3$[30] and Janus group-III chalcogenides.[31,32] The superior properties of Janus structures are due to the out-of-plane symmetry being broken. 2D Ga_2SSe – a member of the Janus group-III chalcogenides – has been predicted to be mechanically and thermodynamically stable at room temperature.[31,32] The electronic and optical properties of Janus Ga_2SSe are dependent on the number of layers,[33] atomic adsorption,[34] and so on.

Currently, making van der Waals heterostructures (vdWHs) from two or more 2DMs is widely used to generate novel properties that may not exist in single-layer forms. Many vdWHs have been constructed and investigated, including the vdWHs based on single-layer BP,[35–38] and based on Janus Ga_2SSe.[39–41] The combination of two or more different semiconducting 2DMs is divided into three different band alignments, including type-I (straddling), type-II (staggered) and type-III (broken). Furthermore, these combinations also lead to an increase in the optical absorption of the constituent 2DMs. With these promising properties, vdWHs are promising competitors for high-performance optoelectronic and photocatalytic applications.[42–44] To date, the combination of single-layer BP and Janus Ga_2SSe monolayers has not yet been constructed and investigated. In this study, we systematically examine the electronic features of BP/Ga_2SSe vdWHs. The influences of the interlayer separations and electric field are also discussed and evaluated. Our findings demonstrated that the BP/Ga_2SSe vdWHs are promising competitors for next-generation multifunctional optoelectronic and photovoltaic devices.

2 Computational methods

All the calculations were based on first-principles calculations and were performed in the Vienna *ab initio* simulation package (VASP).[45] The projector augmented wave (PAW) method[46] with the Perdew-Burke-Ernzerhofer (PBE) functional was used for describing the electron–ion interactions. Moreover, there have been different approaches that described correctly the electron–ion interactions, such as PBEsol[47] and HLE17.[48] The weak vdW interactions in vdWHs were described by adding the Grimme correction in the DFT-D2 method.[49] To avoid the unnecessary interactions, a vacuum thickness of 40 Å was adopted along the z direction of the vdWHs. All atomic structures were fully relaxed until the energy was less than 10^{-6} eV and the forces less than 10^{-3} eV Å^{-1}. The cutoff energy was chosen to be 510 eV and the $(11 \times 11 \times 1)$ k-point meshes were used for the Brillouin zone. The charge density difference in the considered heterostructures was visualized using the VESTA software package.[50] The elastic constants of the considered systems were obtained from the curvature of the energy–strain relationship[51] with suitable sets of deformations in each unit cell. The in-plane elastic constants $[C_{ij}]$ of the materials can be obtained from a stress–strain approach that is based on Hooke's law:[52]

$$\{\delta_{ij}\} = [C_{ij}]\{\varepsilon_{ij}\} \quad (1)$$

where $\{\delta_{ij}\}$ and $\{\varepsilon_{ij}\}$ represent the stress and strain tensors, respectively. The in-plane elastic constants $[C_{ij}]$ are calculated by fitting the parabolic dependence of the energy (E_{tot}) as a function of the strain ε. Thus, the elastic constants C_{11} and C_{22} are obtained from:

$$E_{tot} = \frac{1}{2}C_{11}\varepsilon_{xx}^2 \quad (2)$$

and

$$E_{tot} = \frac{1}{2}C_{22}\varepsilon_{yy}^2 \quad (3)$$

Here, ε_{xx} and ε_{yy} represent the uniaxial strain along the x and y directions, respectively. After that, the elastic constant C_{12} is calculated as follows:

$$E_{tot} = \left(\left(\frac{1}{2}C_{11} + \frac{1}{2}C_{22} + C_{12}\right)\right)\varepsilon_{xx}\varepsilon_{yy} \quad (4)$$

Finally, when the biaxial strain ε_{xy} is applied, we calculated the elastic constant C_{66} as follows:

$$E_{tot} = \frac{1}{2}C_{11}\varepsilon_{xx}^2 + \frac{1}{2}C_{22}\varepsilon_{yy}^2 + C_{12}\varepsilon_{xx}\varepsilon_{yy} + 2C_{66}\varepsilon_{xy}^2 \quad (5)$$

3 Results and discussion

Fig. 1 illustrates the structure of the combination of BP and Ga_2SSe monolayers. The BP/Ga_2SSe heterostructure forms two main stacking patterns of BP/SGa_2Se and BP/SeGa_2S due to the broken vertical symmetry. In the first stacking pattern, the BP layer is stacked on the S layer of the Ga_2SSe layer. Whereas, in the other stacking pattern, the BP is stacked on top of the Se layer of the Ga_2SSe layer. The optimized interlayer separation between BP and Ga_2SSe layers is 3.28 and 3.32 Å for the first and second stacking patterns, respectively. These values of interlayer separation are in the same order of magnitude as those of other BP-based vdWHs,[35,36,38,53] suggesting that the two main stacking patterns of BP/Ga_2SSe vdWHs are typical vdW systems. The binding energy is also taken into account to provide information on the stability of the vdWHs as follows: $E_b = [E_{vdWH} - (E_{BP} + E_{Ga_2SSe})]/A$, where E_{vdWH}, E_{BP} and E_{Ga_2SSe} are the total energies of the vdWH, BP and Ga_2SSe layers, respectively. A

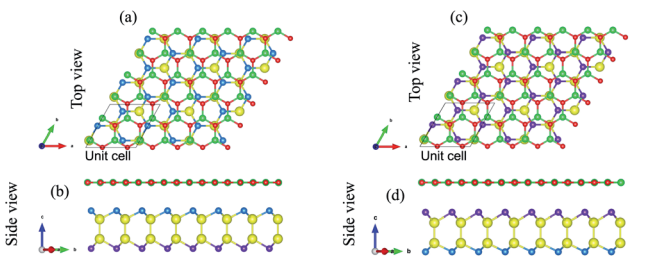

Fig. 1 The optimized atomic structures of (a and b) BP/SGa_2Se and (c and d) BP/SeGa_2S vdWHs. Green and red balls represent the B and P atoms in the BP layer, respectively, while cyan, yellow and violet balls represent the S, Ga and Se atoms in the Janus Ga_2SSe layer, respectively.

is the surface area of the heterostructure. The evaluated E_b of BP/SGa_2Se and BP/$SeGa_2S$ vdWHs is −35.24 and −23.75 meV $Å^{-2}$, respectively. The negative values of E_b suggest that both of these vdWHs are energetically stable. Furthermore, these values of the binding energy of the vdWHs suggest that they are characterized mainly by weak vdW interactions instead of strong covalent bonds. The weak vdW interactions keep the heterostructures feasible and possible to realize experimentally.

The orbital projected band structures (OPBS) of the BP/Ga_2SSe vdWHs for the two stacking patterns are displayed in Fig. 2. One can firstly observe that both stacking patterns of the BP/Ga_2SSe vdWH are semiconductors with direct band gaps. The minimum of the conduction bands (MCB) and the maximum of the valence bands (MVB) are located at the *M* point. More interestingly, both the MCB and MVB of the BP/Ga_2SSe vdWHs for the two stacking patterns originate from the BP layer, which gives rise to formation of the type-I (straddling) band alignment. This finding indicates that the BP/Ga_2SSe vdWH is a suitable material for optoelectronic devices. Furthermore, the band gaps of the BP/SGa_2Se and BP/$SeGa_2S$ vdWHs are about 0.85 eV, which are suitable band gaps for water splitting applications.

The planar-averaged and 3D charge density differences (CDD) are also visualized and displayed in Fig. 3(a) and (b). The CDD can be obtained by the differences between the charge density of the vdWH (ρ_{vdWH}) and those of isolated BP (ρ_{BP}) and Ga_2SSe (ρ_{Ga_2SSe}) as: $\Delta\rho = \rho_{vdWH} - (\rho_{BP} + \rho_{Ga_2SSe})$. The negative sign suggests that the charges are depleted, while the positive sign indicates the charge accumulation. From Fig. 3, the charges are mainly visualized at the interface between the BP layer and the topmost S (Se) layer of the Ga_2SSe layer in their corresponding vdWH. In addition, one can observe that the BP layer gains electrons, while the Ga_2SSe layer donates electrons. Bader charge analysis[54–56] is used to calculate the charge transfers between the two layers in the corresponding vdWHs. The calculated amount of charge transferred between the BP and Ga_2SSe layers in their combined vdWHs is about 0.014 *e*, as depicted in Fig. 3(a and b). The electrostatic potential of the BP/Ga_2SSe vdWH for different stacking patterns is illustrated in Fig. 3(c and d). We observe that the BP layer has a deeper potential than that of the Ga_2SSe layer, indicating that the electrons are transferred from Ga_2SSe to the BP layer.

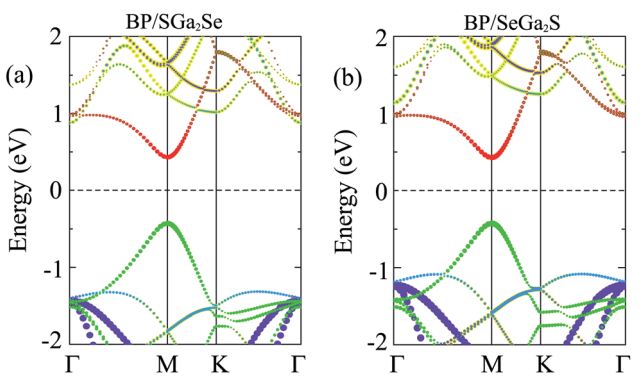

Fig. 2 Orbital projected band structures of the (a) BP/SGa_2Se and (b) BP/$SeGa_2S$ vdWHs. Red and green circles represent the contributions of boron and phosphorus in the BP layer, respectively. Yellow, blue and violet circles represent the contributions of gallium, sulfur and selenium atoms in the Ga_2SSe layer, respectively.

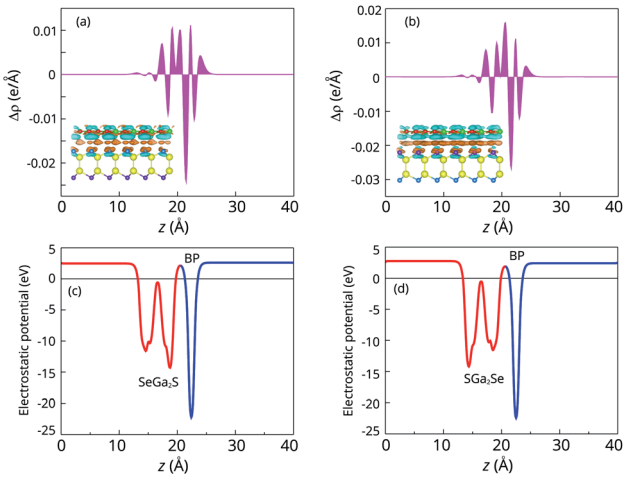

Fig. 3 The planar-averaged charge density difference of the (a) BP/SGa_2Se and (b) BP/$SeGa_2S$ vdWHs. The insets represent the 3D charge density difference. Orange and cyan regions represent the charge accumulation and depletion, respectively. The isosurface value is set to 0.0025 *e* $Å^{-3}$. The electrostatic potential of the (c) BP/SGa_2Se and (d) BP/$SeGa_2S$ heterostructures.

Elastic properties play a crucial role in describing information about the structural stability of any material. We now go on to evaluate the mechanical stability of such systems by calculating their elastic constants, Young's modulus and Poisson's ratio. As we have discussed above, both the BP/SGa_2Se and BP/$SeGa_2S$ vdWHs have layered hexagonal structures. Thus, from eqn (1), there are four independent elastic constants, C_{ij}, of the BP/Ga_2SSe vdWHs, including C_{11}, C_{22}, C_{12} and C_{66}. The measured elastic constants of the BP/Ga_2SSe vdWHs are $C_{11} = C_{22} = 233.30$ N m^{-1}, $C_{12} = 61.50$ N m^{-1} and $C_{66} = (C_{11} - C_{12})/2 = 86$ N m^{-1}. It is clear that these values of the elastic constants meet the Born criteria,[57,58] thus suggesting that the BP/Ga_2SSe vdWHs are mechanically stable. Furthermore, the orientation dependence of Young's modulus and Poisson's ratio of the BP/Ga_2SSe vdWHs is calculated and plotted in Fig. 4. One can find that the Young's modulus and Poisson's ratio of the BP/Ga_2SSe vdWHs for different stacking patterns are about 210 N m^{-1} and 0.25, respectively. One can find that the Young's modulus of the BP/Ga_2SSe vdWHs is still higher than that of single-layer BP,[59] suggesting that the combination of the BP and Ga_2SSe layers gives rise to an enhancement of the Young's modulus.

More interestingly, the electronic and interface characteristics of 2D vdWHs can be modulated by controlling the interlayer separation and applying an electric field.[60–62] We thus consider their influences on the electronic features of the most energetically favorable stacking pattern of the BP/Ga_2SSe vdWHs. The schematic models of the electric field and strain applied to the vdWH are displayed in Fig. S1 of the ESI.† The influence of the electric field (E_{ext}) on the electronic features of the BP/SGa_2Se stacking pattern is displayed in Fig. 5(a). Under the

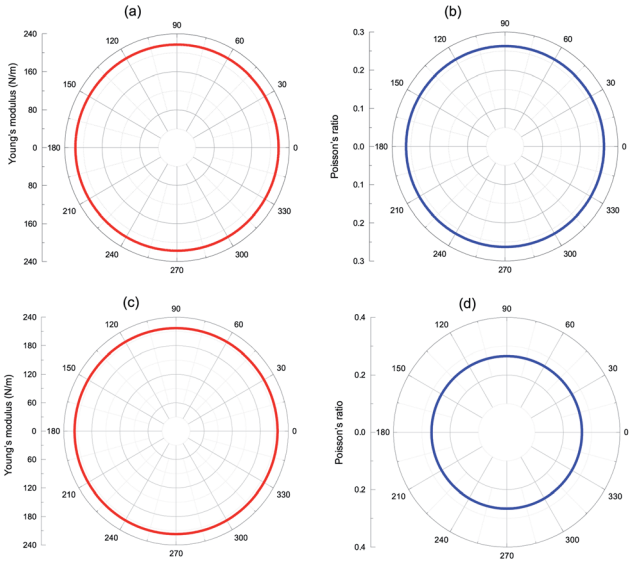

Fig. 4 Polar plots of (a and c) Young's modulus and (b and d) Poisson's ratio of the (a and b) BP/SGa_2Se and (c and d) BP/$SeGa_2S$ stacking patterns.

negative neg-E_{ext}, the MVB of the BP and Ga_2SSe layers shifts in opposite directions. The MVB of the BP layer comes to the Fermi level (E_F), while the MVB of the Ga_2SSe layer shifts far from the E_F. At the same time, the MCB of the BP and Ga_2SSe layers also moves in different directions. The MCB of the BP layer shifts far from the E_F, whereas the MCB of the Ga_2SSe layer comes towards the E_F. Owing to these movements, at the critical strength of neg-$E_{ext} = -0.40$ V nm^{-1}, the MCB of the Ga_2SSe layer moves closer to the E_F than that of the BP layer. In this case, the MCB of the BP/Ga_2SSe vdWH originates from the Ga_2SSe layer, while the MVB is preserved by the contribution of the BP layer, thus revealing the conversion from a type-I to type-II (staggered) band alignment. It is obvious that the type-II band alignment reduces the recombination of electron–hole pairs, revealing that the BP/Ga_2SSe vdWH is beneficial for photovoltaic devices. The influence of the positive pos-E_{ext} on the electronic features of the BP/Ga_2SSe vdWH is illustrated in Fig. 5(b). One can observe that the MVB of the Ga_2SSe layer tends to shift towards the E_F. At the same time, the MVB of the BP layer is shifted closer to the E_F. At the critical strength of pos-$E_{ext} = +0.40$ V nm^{-1}, the MVB of the BP layer touches the E_F. Furthermore, when pos-E_{ext} is further increased to +0.5 V nm^{-1}, the MVB of the BP layer crosses the Fermi level, resulting in the transformation from semiconductor to metal, as depicted in Fig. S2 of the ESI.† All of the above-discussed findings indicate that E_{ext} gives rise to the conversion from type-I to type-II band alignment and the transformation from semiconductor to metal in the BP/Ga_2SSe vdWH.

The influence of the interlayer separation on the electronic features of the BP/Ga_2SSe vdWH is illustrated in Fig. 6. The change of the interlayer separation is defined as $\Delta D = D_0 - D$, where D_0 and D represent the interlayer separation of the BP/Ga_2SSe vdWH in the equilibrium state and strained state, respectively. Under the compressive separation, *i.e.* $\Delta D < 0$, as depicted in Fig. 6(a), it tends to a reduction of the band gap of the BP/Ga_2SSe vdWH. The band gap of the BP/Ga_2SSe vdWH reduces from 0.85 eV at $\Delta D = 0$ to 0.67 and 0.45 eV at $\Delta D = -0.8$

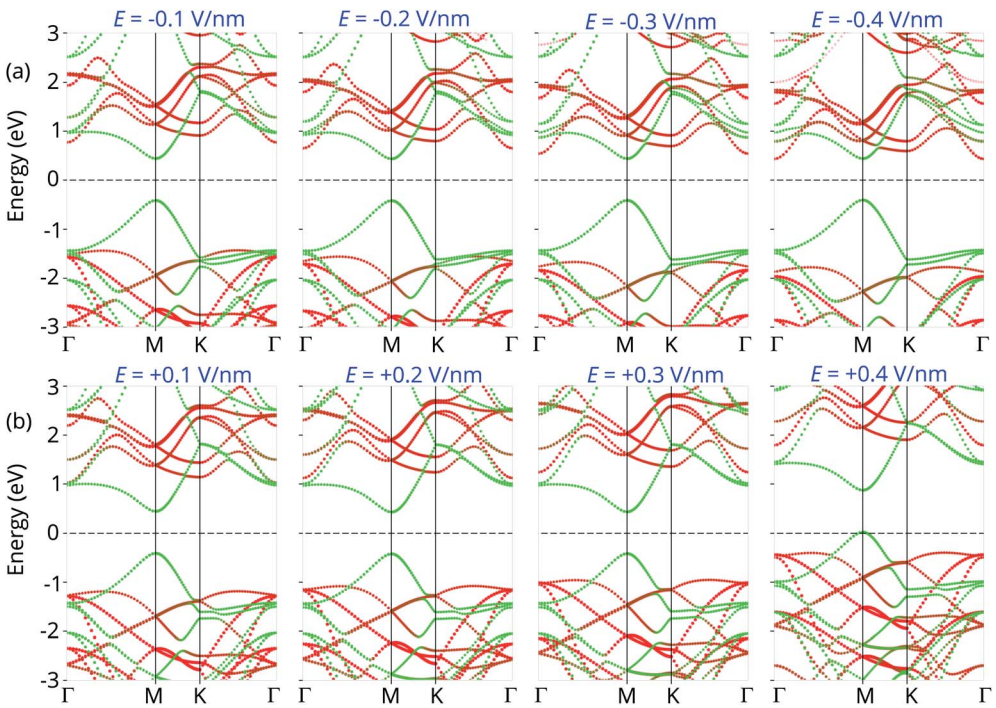

Fig. 5 Projected band structures of the BP/SGa_2Se vdWH under (a) negative and (b) positive electric fields. Green and red lines represent the contributions of the BP and Ga_2SSe layers, respectively. The Fermi level is set to be zero and defined by the dashed line.

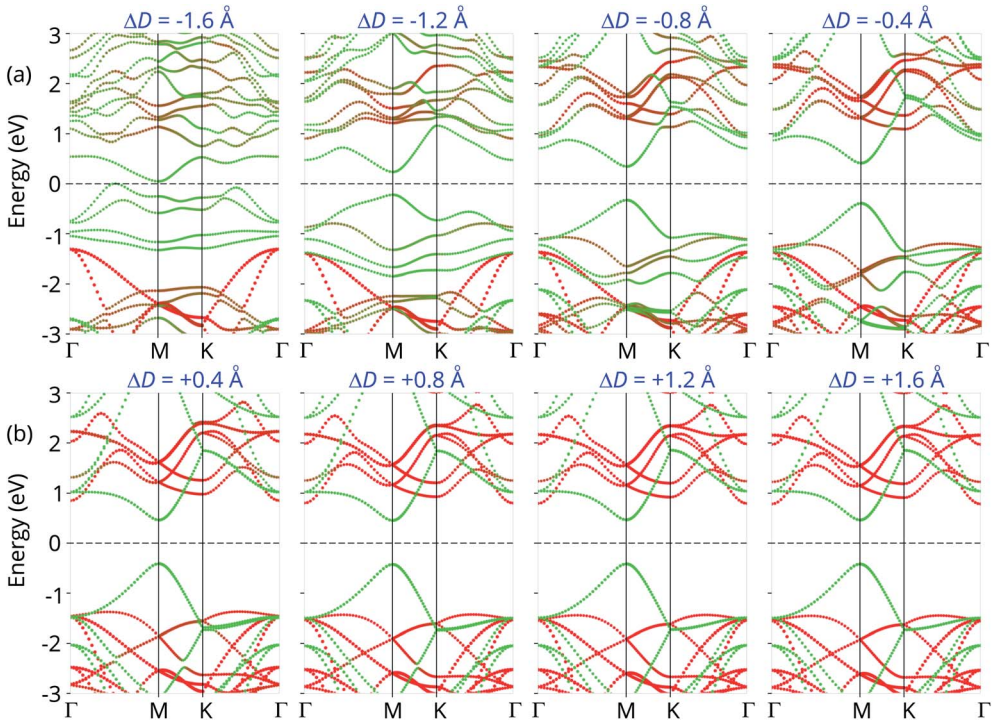

Fig. 6 Projected band structures of the BP/SGa$_2$Se heterostructure under (a) compressive and (b) tensile strains. Green and red lines represent the contributions of the BP and Ga$_2$SSe layers, respectively. The Fermi level is set to be zero and defined by the dashed line.

Å and −1.2 Å, respectively. The BP/Ga$_2$SSe vdWH at $\Delta D <$ 0 maintains the type-I band alignment with both the MCB and MVB originating from the BP layer. At $\Delta D = -1.6$ Å, both the MVB and MCB of the BP layer in the BP/Ga$_2$SSe vdWH touch the E_F. In particular, at $\Delta D = -1.7$ Å, as depicted in Fig. S2 of the ESI,† both the MVB and MCB of the heterostructure cross the Fermi level, suggesting that the BP/Ga$_2$SSe vdWH turns into a metal. Whereas with an increase of the interlayer separation, *i.e.* $\Delta D > 0$, the band edges of both the BP and Ga$_2$SSe layers in the BP/Ga$_2$SSe vdWH are almost unchanged in comparison with the position of the E_F. This finding indicates that the BP/Ga$_2$SSe vdWH keeps the type-I band alignment with the contributions of the BP layer in both the MVB and MCB.

4 Conclusions

In summary, we have investigated the electronic structure and interface characteristics of vdWHs combining single-layer BP and Janus Ga$_2$SSe using first-principles calculations. Owing to the out-of-plane symmetry being broken in the Janus Ga$_2$SSe layer, the BP/Ga$_2$SSe vdWHs form two different stacking patterns, BP/SGa$_2$Se and BP/SeGa$_2$S. Both these stacking patterns are energetically and mechanically stable, confirming that they can be obtained experimentally. Moreover, the combination of single-layer BP and Janus Ga$_2$SSe tends to an enhancement of the elastic constants, as well as the Young's modulus, compared to the constituent monolayers. The BP/Ga$_2$SSe vdWHs for the two stacking patterns exhibit type-I band alignment with both the MVB and MCB originating from the BP layer. Interestingly, we found that the electronic structure and contact types of the BP/Ga$_2$SSe vdWHs are dependent on the interlayer separation and electric field, giving rise to the conversion from type-I to type-II band alignment, and from semiconductor to metal. Our results indicate that the BP/Ga$_2$SSe vdWH would be appropriate for next-generation multifunctional optoelectronic and photovoltaic devices.

Conflicts of interest

There are no conflicts to declare.

References

1 S. Z. Butler, S. M. Hollen, L. Cao, Y. Cui, J. A. Gupta, H. R. Gutiérrez, T. F. Heinz, S. S. Hong, J. Huang, A. F. Ismach, E. Johnston-Halperin, M. Kuno, V. V. Plashnitsa, R. D. Robinson, R. S. Ruoff, S. Salahuddin, J. Shan, L. Shio, M. G. Spencer, M. Terrones, W. Windl and J. E. Goldberger, *ACS Nano*, 2013, **7**, 2898–2926.
2 P. Miró, M. Audiffred and T. Heine, *Chem. Soc. Rev.*, 2014, **43**, 6537–6554.
3 K. S. Novoselov, A. K. Geim, S. V. Morozov, D.-e. Jiang, Y. Zhang, S. V. Dubonos, I. V. Grigorieva and A. A. Firsov, *Science*, 2004, **306**, 666–669.
4 X. Du, I. Skachko, A. Barker and E. Y. Andrei, *Nat. Nanotechnol.*, 2008, **3**, 491–495.

5 K. S. Novoselov, A. K. Geim, S. V. Morozov, D. Jiang, M. I. Katsnelson, I. Grigorieva, S. Dubonos and a. Firsov, *Nature*, 2005, **438**, 197–200.
6 D. Reddy, L. F. Register, G. D. Carpenter and S. K. Banerjee, *J. Phys. D: Appl. Phys.*, 2011, **44**, 313001.
7 T. Wehling, K. Novoselov, S. Morozov, E. Vdovin, M. Katsnelson, A. Geim and A. Lichtenstein, *Nano Lett.*, 2008, **8**, 173–177.
8 T. Kuila, S. Bose, A. K. Mishra, P. Khanra, N. H. Kim and J. H. Lee, *Prog. Mater. Sci.*, 2012, **57**, 1061–1105.
9 S. Y. Zhou, G.-H. Gweon, A. Fedorov, P. N. First, W. De Heer, D.-H. Lee, F. Guinea, A. Castro Neto and A. Lanzara, *Nat. Mater.*, 2007, **6**, 770–775.
10 A. Carvalho, M. Wang, X. Zhu, A. S. Rodin, H. Su and A. H. Castro Neto, *Nat. Rev. Mater.*, 2016, **1**, 16061.
11 S. Manzeli, D. Ovchinnikov, D. Pasquier, O. V. Yazyev and A. Kis, *Nat. Rev. Mater.*, 2017, **2**, 17033.
12 Y. Gogotsi and B. Anasori, *The rise of MXenes*, 2019.
13 M. Khazaei, A. Mishra, N. S. Venkataramanan, A. K. Singh and S. Yunoki, *Curr. Opin. Solid State Mater. Sci.*, 2019, **23**, 164–178.
14 Y. Kumashiro, K. Nakamura, T. Enomoto and M. Tanaka, *J. Mater. Sci.: Mater. Electron.*, 2011, **22**, 966–973.
15 K. Shohno, M. Takigawa and T. Nakada, *J. Cryst. Growth*, 1974, **24–25**, 193–196.
16 Y. Wang, C. Huang, D. Li, P. Li, J. Yu, Y. Zhang and J. Xu, *J. Phys.: Condens. Matter*, 2019, **31**, 285501.
17 Y. Wang, C. Huang, D. Li, F. Huang, X. Zhang, K. Huang and J. Xu, *J. Phys.: Condens. Matter*, 2019, **31**, 465502.
18 H. Şahin, S. Cahangirov, M. Topsakal, E. Bekaroglu, E. Akturk, R. T. Senger and S. Ciraci, *Phys. Rev. B: Condens. Matter Mater. Phys.*, 2009, **80**, 155453.
19 R. Zhang, F. Sun, Z. Zhang, J. Liu, Y. Tian, Y. Zhang, X. Wei, T. Guo, J. Fan, L. Ni, et al., *Appl. Surf. Sci.*, 2021, **535**, 147825.
20 M. Xie, S. Zhang, B. Cai, Z. Zhu, Y. Zou and H. Zeng, *Nanoscale*, 2016, **8**, 13407–13413.
21 K. I. Bolotin, K. J. Sikes, Z. Jiang, M. Klima, G. Fudenberg, J. Hone, P. Kim and H. Stormer, *Solid State Commun.*, 2008, **146**, 351–355.
22 M. M. Obeid, H. R. Jappor, K. Al-Marzoki, D. Hoat, T. V. Vu, S. J. Edrees, Z. M. Yaseen and M. M. Shukur, *Comput. Mater. Sci.*, 2019, **170**, 109201.
23 B. Onat, L. Hallioglu, S. Ipek and E. Durgun, *J. Phys. Chem. C*, 2017, **121**, 4583–4592.
24 M. Yarmohammadi and K. Mirabbaszadeh, *J. Appl. Phys.*, 2020, **128**, 215703.
25 J. Zhang, S. Jia, I. Kholmanov, L. Dong, D. Er, W. Chen, H. Guo, Z. Jin, V. B. Shenoy, L. Shi, et al., *ACS Nano*, 2017, **11**, 8192–8198.
26 A.-Y. Lu, H. Zhu, J. Xiao, C.-P. Chuu, Y. Han, M.-H. Chiu, C.-C. Cheng, C.-W. Yang, K.-H. Wei, Y. Yang, *et al.*, *Nat. Nanotechnol.*, 2017, **12**, 744–749.
27 S.-D. Guo, Y.-F. Li and X.-S. Guo, *Comput. Mater. Sci.*, 2019, **161**, 16–23.
28 R. Peng, Y. Ma, B. Huang and Y. Dai, *J. Mater. Chem. A*, 2019, **7**, 603–610.
29 X. Gao, Y. Shen, J. Liu, L. Lv, M. Zhou, Z. Zhou, Y. P. Feng and L. Shen, *J. Mater. Chem. C*, 2021, **9**, 15026–15033.
30 Y. Luo, M. Sun, J. Yu and U. Schwingenschlogl, *Chem. Mater.*, 2021, **33**, 4128–4134.
31 R. da Silva, R. Barbosa, R. R. Mancano, N. Duraes, R. B. Pontes, R. Miwa, A. Fazzio and J. E. Padilha, *ACS Appl. Nano Mater.*, 2019, **2**, 890–897.
32 Y. Guo, S. Zhou, Y. Bai and J. Zhao, *Appl. Phys. Lett.*, 2017, **110**, 163102.
33 A. Huang, W. Shi and Z. Wang, *J. Phys. Chem. C*, 2019, **123**, 11388–11396.
34 S. Singh and S. Choudhary, *Opt. Quantum Electron.*, 2021, **53**, 1–13.
35 C. Nguyen, N. V. Hoang, H. V. Phuc, A. Y. Sin and C. V. Nguyen, *J. Phys. Chem. Lett.*, 2021, **12**, 5076–5084.
36 I. Shahid, S. Ahmad, N. Shehzad, S. Yao, C. V. Nguyen, L. Zhang and Z. Zhou, *Appl. Surf. Sci.*, 2020, **523**, 146483.
37 J. Li, H. Duan, B. Zeng, Q. Jing, B. Cao, F. Chen and M. Long, *J. Phys. Chem. C*, 2018, **122**, 26120–26129.
38 A. Mogulkoc, Y. Mogulkoc, M. Modarresi and B. Alkan, *Phys. Chem. Chem. Phys.*, 2018, **20**, 28124–28134.
39 H. T. Nguyen, M. M. Obeid, A. Bafekry, M. Idrees, T. V. Vu, H. V. Phuc, N. N. Hieu, L. T. Hoa, B. Amin and C. V. Nguyen, *Phys. Rev. B*, 2020, **102**, 075414.
40 W. Zhang, Y. Yin and C. He, *J. Phys. Chem. Lett.*, 2021, **12**, 5064–5075.
41 L. Hu and D. Wei, *J. Phys. Chem. C*, 2018, **122**, 27795–27802.
42 B. Luo, G. Liu and L. Wang, *Nanoscale*, 2016, **8**, 6904–6920.
43 P. Garg, S. Kumar, I. Choudhuri, A. Mahata and B. Pathak, *J. Phys. Chem. C*, 2016, **120**, 7052–7060.
44 A. Singh, M. Jain and S. Bhattacharya, *Nanoscale Adv.*, 2021, **3**, 2837–2845.
45 G. Kresse and J. Hafner, *Phys. Rev. B: Condens. Matter Mater. Phys.*, 1993, **47**, 558.
46 J. P. Perdew, K. Burke and M. Ernzerhof, *Phys. Rev. Lett.*, 1996, **77**, 3865.
47 J. P. Perdew, A. Ruzsinszky, G. I. Csonka, O. A. Vydrov, G. E. Scuseria, L. A. Constantin, X. Zhou and K. Burke, *Phys. Rev. Lett.*, 2008, **100**, 136406.
48 I. Choudhuri and D. G. Truhlar, *J. Phys. Chem. C*, 2019, **123**, 17416–17424.
49 S. Grimme, *J. Comput. Chem.*, 2006, **27**, 1787–1799.
50 K. Momma and F. Izumi, *J. Appl. Crystallogr.*, 2008, **41**, 653–658.
51 E. Cadelano, P. L. Palla, S. Giordano and L. Colombo, *Phys. Rev. B: Condens. Matter Mater. Phys.*, 2010, **82**, 235414.
52 S. Shang, G. Sheng, Y. Wang, L. Chen and Z. Liu, *Phys. Rev. B: Condens. Matter Mater. Phys.*, 2009, **80**, 052102.
53 Y. Mogulkoc, R. Caglayan and Y. Ciftci, *Phys. Rev. Appl.*, 2021, **16**, 024001.
54 W. Tang, E. Sanville and G. Henkelman, *J. Phys.: Condens. Matter*, 2009, **21**, 084204.
55 G. Henkelman, A. Arnaldsson and H. Jónsson, *Comput. Mater. Sci.*, 2006, **36**, 354–360.
56 E. Sanville, S. D. Kenny, R. Smith and G. Henkelman, *J. Comput. Chem.*, 2007, **28**, 899–908.
57 M. Born, K. Huang and M. Lax, *Am. J. Phys.*, 1955, **23**, 474.

58 F. Mouhat and F.-X. Coudert, *Phys. Rev. B: Condens. Matter Mater. Phys.*, 2014, **90**, 224104.
59 T. V. Vu, A. Kartamyshev, N. V. Hieu, T. D. Dang, S.-N. Nguyen, N. Poklonski, C. V. Nguyen, H. V. Phuc and N. N. Hieu, *RSC Adv.*, 2021, **11**, 8552–8558.
60 X. Li, G. Jia, J. Du, X. Song, C. Xia, Z. Wei and J. Li, *J. Mater. Chem. C*, 2018, **6**, 10010–10019.
61 X. Gao, Y. Shen, Y. Ma, S. Wu and Z. Zhou, *Carbon*, 2019, **146**, 337–347.
62 B. Sun, Y.-F. Ding, P.-B. He, Y.-Q. Zhao and M.-Q. Cai, *Phys. Rev. Appl.*, 2021, **16**, 044003.